AGU100 ADVANCING EARTH AND SPACE SCIENCE

JGR

Journal of Geophysical Research: Space Physics

RESEARCH ARTICLE
10.1029/2017JA024980

Key Points:
- Characteristics of premidnight and postmidnight plasma irregularities are studied over India
- Results suggest that while postsunset ESF is linked mostly to the equatorial process, a few of the postmidnight ESFs could be linked to the nonequatorial process
- Persistence of equinoctial asymmetry in the plasma irregularities for several years

Correspondence to:
S. Sripathi,
ssripathi.iig@gmail.com

Citation:
Sripathi, S., Sreekumar, S., & Banola, S. (2018). Characteristics of equatorial and low-latitude plasma irregularities as investigated using a meridional chain of radio experiments over India. *Journal of Geophysical Research: Space Physics*, *123*, 4364–4380. https://doi.org/10.1029/2017JA024980

Received 8 NOV 2017
Accepted 10 MAY 2018
Accepted article online 17 MAY 2018
Published online 28 MAY 2018

Characteristics of Equatorial and Low-Latitude Plasma Irregularities as Investigated Using a Meridional Chain of Radio Experiments Over India

S. Sripathi[1], **Sreeba Sreekumar**[1], **and S. Banola**[1]

[1]Indian Institute of Geomagnetism, Navi Mumbai, India

Abstract The characteristics of equatorial and low-latitude plasma irregularities are studied using a meridional chain of ionosondes located at Tirunelveli, Hyderabad, and Allahabad and Global Positioning System (GPS) receivers located at Tirunelveli, Mumbai, and Nagpur during the year 2015. The observations suggest that while stronger and longer duration of equatorial spread *F* irregularities occur in the postsunset sector during equinoxes and winter, they occur mostly in the postmidnight sector during summer, while being weaker in strength and shorter in duration. Further, the postsunset spread *F* occurs first at the equator followed by their occurrence at low latitudes during equinoxes and winter, while the postmidnight spread *F* during summer are found to be stronger and earlier at low latitudes followed by their occurrence at the equator. While plasma irregularities are observed by both the ionosondes and GPS receivers during both equinoxes and winter, it is observed mostly by the ionosondes during summer. The results further strengthen the view that while postsunset spread *F* in equinoxes and winter are generated by the equatorial processes, postmidnight spread *F* in the summer may be linked to the nonequatorial processes. The results also reemphasize the asymmetric distribution of plasma irregularities or scintillations during equinoxes wherein vernal (autumn) equinox shows more intense plasma irregularities than autumn (vernal) equinox during certain years. Also, using a larger data set of simultaneous GPS and ionosonde observations, the relationship of prereversal enhancement and strength of L-band scintillations with solar flux, Kp index, and equatorial electrojet strength are examined.

Plain Language Summary It is known that nighttime equatorial ionosphere affects the radio wave communication due to presence of electron density fluctuations often known as plasma irregularities. These irregularities are observed by variety of ground- and space-based instruments. These plasma irregularities have large variability due to forcing from the above and below. Due to advent of Global Positioning System (GPS) receivers, ionospheric scintillations caused by these plasma irregularities are used extensively to monitor them under varied space weather conditions. While GPS receivers monitor the scintillations, which are integrated quantity, ionosondes provide information about the altitude variation of ionospheric layers. Accordingly, uniqueness of this work lies in the integration of these two observations to bring morphological differences between these two scales and their general characteristics during different seasons over Indian equatorial and low-latitude stations using chain of ionosondes and GPS receivers. Interestingly, the postmidnight spread *F* during summer is found to be stronger and earlier at low latitudes followed by their occurrence at the equator. The results further strengthen the view that while postsunset spread *F* in equinoxes and winter are generated by the equatorial processes, postmidnight spread *F* in the summer may be linked to the nonequatorial processes.

1. Introduction

Nocturnal variation of equatorial spread *F* (ESF) irregularities have been studied extensively by radio, optical, and in situ techniques (e.g., Basu et al., 1978; Fejer & Kelley, 1980; Kelley et al., 2011). These plasma irregularities are believed to be generated by the Rayleigh-Taylor (RT) instability process at the bottomside of the *F* layer, and they grow nonlinearly to the topside of the *F* region (Fejer & Kelley, 1980; Kelley et al., 2011, and references therein). As they grow nonlinearly to higher altitudes, they also map to higher latitudes on either side of the magnetic equator. They produce intense L-band scintillations in the equatorial ionization anomaly (EIA) region due to the presence of large density gradients (e.g., Ray & DasGupta, 2007). In the presence of these plasma irregularities, radio waves that traverse through the ionosphere undergo radio scintillations, a key concern of communication and navigation community. These irregularities are correlated well with

the solar flux and the geomagnetic activity (Abdu, 2001; Buhari et al., 2017; Chandra & Rastogi, 1972; Gentile et al., 2006; Huang et al., 2002; Rastogi, 1980; Ray & DasGupta, 2007). Though many aspects of these irregularities have been understood by now, still key issues like day-to-day and intraseasonal variabilities of these irregularities are yet to be realized (e.g., Kelley et al., 2011). It is now realized that in addition to the equatorial plasma drifts, several other key factors play an important role in causing these variabilities.

Among many of the key factors, gravity waves, longitudinal gradient in the field line integrated conductivity of the *E* and *F* regions, crest to trough ratio, and evening vortex are believed to play a major role in the generation of these plasma irregularities (e.g., Abdu, 2001; Abdu et al., 2009; Burke et al., 2004). As the symmetric EIA crests with reference to the magnetic equator enhance the ESF activity, the asymmetric EIA crests about the magnetic equator suppress the ESF activity. Similarly, when the conjugate *E* regions simultaneously undergo sunset, ESF activity is enhanced. Accordingly, the plasma irregularities are generated during equinoxes in India when the conjugate *E* regions simultaneously undergo sunset. Over the equator, the *F* region dynamo takes over the *E* region dynamo through the *F* region zonal winds in the evening sector. The altitude variation of these zonal winds suggests that they are westward in the bottomside of *F* region, but as height increases, they flow eastward (e.g., Rodrigues et al., 2012). Now it is evident that such strong zonal shears exist in the equatorial *F* region during the postsunset hours where the plasma flow reverses its direction (known as evening vortex), which is believed to be responsible for the seed perturbation required for the generation of plasma irregularities (Kudeki & Bhattacharyya, 1999). Model simulations of the evening vortex suggest that both the *E* and *F* region dynamos are important for the evening vertical shear in the zonal plasma drifts, which are responsible for the evening vortex (Rodrigues et al., 2012). Another mechanism suggests that the large-scale wave structures in the zonal direction are necessary at the bottomside of the *F* layer during the sunset for the generation of ESF irregularities (e.g., Tsunoda & Ecklund, 2007). Anomalous postsunset height rise of the *F* layer in the equator on some occasions is also suggested to be due to the prevailing *F* region dynamo in the dusk sector (Sastri, 1998). Similarly, many investigators have examined the role of conductivities of the *E* and *F* regions and Es layers at low latitudes on the development of ESF by modifying the flux tube-integrated conductivities (e.g., Abdu et al., 2003; Stephan et al., 2002).

The above theoretical understanding has come from the ESF irregularities, which are observed mostly at the postsunset hours. Now it is known that the ESF irregularities are not only predominant in the postsunset sector during equinoxes and winter but also occur during summer in the postmidnight sector (e.g., Li et al., 2012; Patra et al., 2009). The plasma irregularities in the postsunset sector are prominent during high solar activity periods, while they are dominant in the postmidnight sector during low solar activity period. There is a renewed interest in the recent times to understand the differences between these two types of plasma irregularities. The causes for postmidnight spread *F* during summer season have not yet been established well. In fact, the observations of postmidnight spread *F* during summer are relatively rare due to its weak strength and less frequency, which is contrary to the postsunset plasma irregularities. Over the Indian region, Chandra and Rastogi (1972), Sastri et al. (1997), and Subbarao and Murthy (1994) have made some studies during summer season to understand their characteristics. The prolonged low solar activity period during 2007–2009 in the recent past generated new interest among many investigators to examine them thoroughly. Since the Es layers are common and strong during summer season at low latitudes, it is suggested that the polarization electric fields generated in the Es layers may map to the *F* region and produce Perkins type instability (Tsunoda, 2007). Patra et al. (2009) have investigated the radar echoes using very high frequency radar at Gadanki during summer season under such extreme low solar activity period and suggested that the postmidnight irregularities in the summer could be generated by the gradient drift-assisted RT instability since there is no other evidence that these irregularities could be generated in the postmidnight period. The plasma irregularities that are studied using C/NOFS satellite data are also found to occur more frequently in the postmidnight sector than in the postsunset sector during the low solar activity period (Dao et al., 2011). Yizengaw et al. (2013) have studied the postmidnight plasma bubbles and scintillations and their relation to strong occurrence of Es layers during summer. They pointed out that the strong occurrence of Es layers in the summer could explain the incidence of large number of postmidnight bubbles in the African sector.

In the present paper, we present the characteristics of ionospheric plasma irregularities occurring at postmidnight and postsunset sectors during equinoxes, winter season, and summer season in India and their variabilities as observed using a chain of ionosondes along with the data from GPS receivers during the year 2015, a

moderate solar flux year. This is for the first time we use a network of ionosondes and GPS receivers located right from the equator to the low latitudes to investigate the characteristics of the equatorial plasma irregularities vis-à-vis low-latitude type plasma irregularities. In addition, we also utilize the observations of ionosonde and L-band scintillations over Tirunelveli (TIR), an equatorial station for nearly one solar cycle to study its relation to solar flux besides various other relations.

2. Details of the Experimental Setup and its Database

We analyzed data from a chain of Canadian Advanced Digital Ionosondes (CADI) located at equatorial and low-latitude stations in India, namely, TIR/Hyderabad/Allahabad during the year 2015. Many researchers across the globe use the CADI ionosondes for their research work (e.g., MacDougall et al., 1995). Uninterrupted operations were conducted using these ionosondes to investigate the low-latitude ionospheric electrodynamics under quiet and disturbed periods for a few years. While it is operated at 10-min interval at TIR and Hyderabad, it is also operated at 15 and 5 min intervals at Allahabad during the year 2015. Massive task of manual scaling of the CADI ionosonde data at all the stations is carried out. Simultaneously, GPS/GNSS receivers located at TIR, Mumbai, and Nagpur stations are analyzed to examine the latitudinal variation of total electron content (TEC)/L-band scintillations. Appropriate mapping function, $S_f = \cos\chi$ is used, that is, VTEC = STEC * S_f or VTEC = STEC * $\cos\chi$ to convert slant TEC to vertical TEC. Here $\chi = \sin^{-1}\left[\frac{R_E \cos\alpha}{R_E+h}\right]$, a is the elevation angle at Ionospheric Penetration Point (IPP), R_E = 6378 km, and h = 350 km. We also analyzed long series of GPS SCINDA (scintillation network decision aid) data over TIR during the years 2007–2015 to study the GPS TEC and L-band scintillations. The rate of TEC index (ROTI), which is a proxy for the electron density fluctuations in the ionosphere, is obtained using the technique described by Pi et al. (1997), which can be represented mathematically as $\sqrt{<\mathrm{ROT}^2> - <\mathrm{ROT}>^2}$, where ROT is rate of change in TEC in TEC units/minute. Equatorial electrojet (EEJ) strength is obtained by subtracting the horizontal component (ΔH) of geomagnetic field measurements made at TIR (equator) and Alibag (low latitude) using fluxgate magnetometers during the same period to identify its role and its relation to ESF irregularities. Similarly, we have obtained solar and geomagnetic indices data for the same period to study their relations.

3. Observations and Data Analysis

In this section, we present the integrated characteristics of the spread *F* irregularities at TIR, Hyderabad, and Allahabad stations using ionosondes along with ROTI and L-band scintillations as obtained from TIR, Mumbai, and Nagpur stations. The ESF irregularities usually follow power law where large-scale structures occur first and small-scale irregularities are believed to be generated on the western walls of these large-scale structures (Fejer & Kelley, 1980). Accordingly, the irregularities as seen in ionosondes, L-band scintillations, and ROTI as calculated from TEC represent different scale sizes of the irregularity spectrum. While ionosondes represent scale sizes of few hundreds of kilometers, ROTI represents few tens of kilometers. But L-band scintillations are caused by intermediate scale size of irregularities of ~400 m. Accordingly, large-scale structures occur first followed by smaller scale irregularities but smaller scale irregularities disappear first followed by large-scale structures, though there could be some deviations from these general behavior (e.g., Basu et al., 1978; Sripathi et al., 2008). So the morphological characteristics of these irregularities as presented here also represent the irregularities of those scales only. Here we also present their various correlations with solar and geomagnetic activity strengths using larger data set of GPS receiver and ionosondes. Table 1 shows the various instruments used in the present analysis and their coordinates. Figures 1a and 1b depict (a) location of various instruments and (b) field line geometry connecting apex altitude with various latitudes through uniform magnetic flux density using dipolar magnetic configuration, respectively.

3.1. GPS L-Band Scintillations, ROTI Along With Equatorial Spread *F* (ESF) Occurrence During 2007–2015

Figures 2a–2d show the temporal and seasonal variations of S4 index and ROTI index as obtained from GPS SCINDA receiver at TIR and monthly % occurrence of spread *F* using CADI ionosonde at TIR along with mean monthly solar flux for the years 2007–2015 (~10 years). Figure 2a shows the solar flux values, while Figure 2b

Table 1
List of Ground Stations Used in the Present Study

Station	Instrument	Geog. latitude and longitude	Geomag. latitude
Tirunelveli (TIR)	CADI ionosonde, GPS receiver, geomagnetic data	8.73°N, 77.7°E	0.23°N
Hyderabad (HYD)	CADI ionosonde	17.36°N, 78.47°E	8.76°N
Mumbai (MUM)	GNSS receiver	19.07°N, 72.88°E	10.89°N
Nagpur (NGP)	GNSS receiver	21.14°N, 79.08°E	12.42°N
Allahabad (ALD)	CADI ionosonde	25.43°N, 81.84°E	16.48°N
Alibag (ABG)	Geomagnetic data	18.62°N, 72.87°E	10.36°N

shows the S4 index and Figure 2c the mean ROTI. Here *y* axis for Figures 2b and 2c indicates time (IST [Indian Standard Time]), which is advanced by 05:30 to UT time. Figure 2d shows the monthly % occurrence of spread *F* using CADI ionosonde during 2008–2015. Here the monthly % occurrence of spread *F* in ionosonde is calculated based on the ratio between number of spread *F* days to total number of days in that month which is multiplied by 100 to get occurrence percentage. The color code indicates (a) strength of S4 index and (b) mean values of ROTI. Here the S4 index and ROTI values are averaged for every 10-min interval before plotting. As can be seen in the Figure 2a, while the mean monthly solar flux at F10.7 cm is varied between ~60 and 70 solar flux unit (sfu; 1 sfu = $10^{-22} \cdot \mathrm{Wm}^{-2} \cdot \mathrm{Hz}^{-1}$) in the low solar activity years, that is, 2007–2010, they are steadily varied between 90 and 150 sfu in the moderate to high solar activity years, that is, 2011–2015. The S4 index and ROTI as shown in the plots during the years 2007 to 2015 indicate that no scintillations to very weak scintillations were observed during low solar activity period, while they were slowly enhanced as solar activity increases. The results also suggest that both S4 index and ROTI were strong during equinoxes followed by winter and summer seasons. The monthly % occurrence of spread *F* in Figure 2d indicates that it varied mostly $<$50% during 2008–2009 (except few months); spread *F* occurrence during 2010–2015 suggests that they are observed very strong during equinoxes and winter followed by summer. Closer look at these plots suggests that occurrence of spread *F* or scintillations are skewed during equinoxes. The observations reveal that vernal equinox had strong scintillations/ESF when compared with autumn equinox for few years (e.g., 2014 and 2015), which is in contrast with other years where autumn equinox had strong scintillations/ESF (e.g., 2011 and 2012). Such asymmetry of scintillations/ESF occurrence was seen for several other years as well where asymmetry shifts from one equinox to other. While it is known that solar flux has a role to play, only flux differences cannot

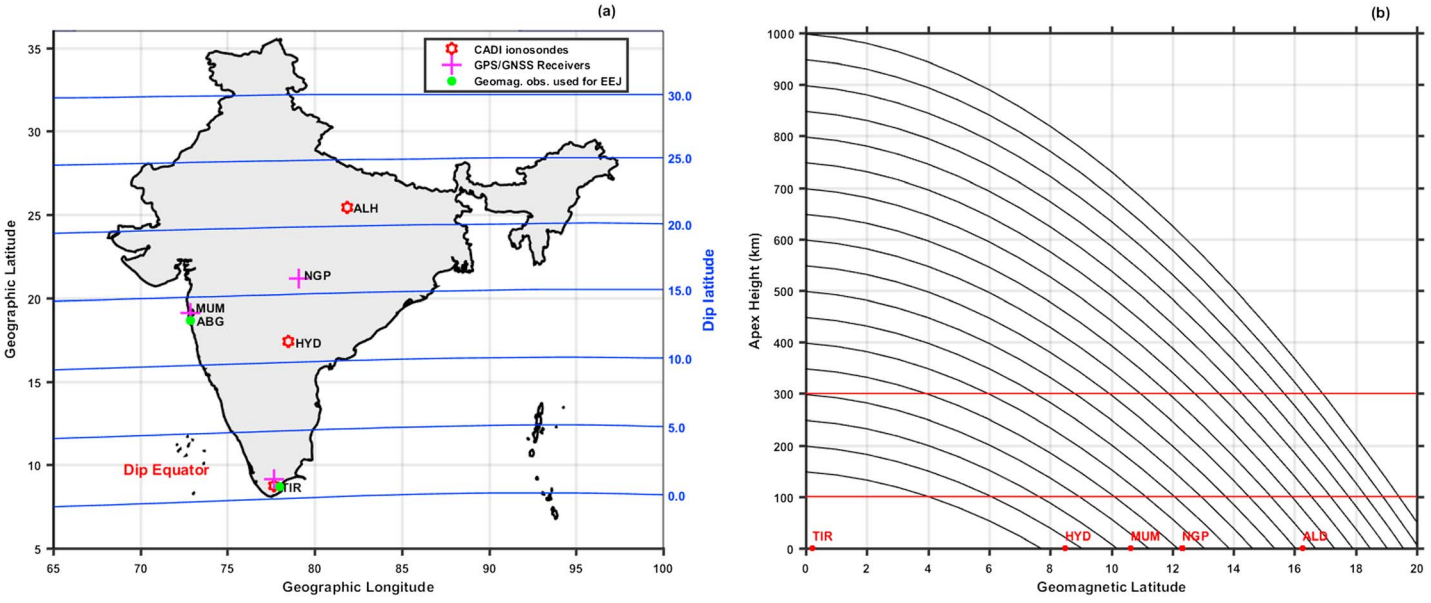

Figure 1. (a and b) The location map of various instruments used in the present analysis. Figure 1b shows the altitude-latitude relation of flux tube geometry. Here the "red" lines indicate dipole field line of different latitudes connecting to 100 and 300 km apex altitudes.

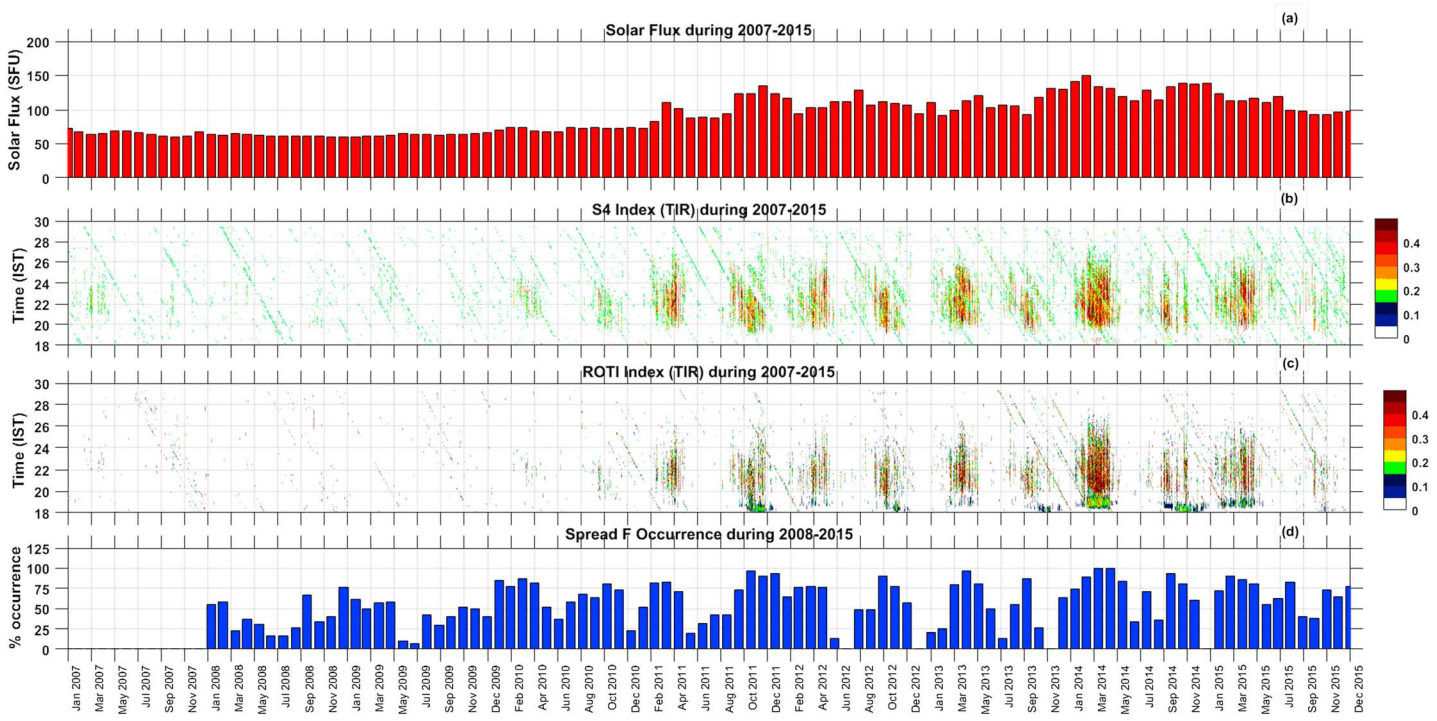

Figure 2. (a) The monthly mean solar flux for the years 2007–2015. The daily temporal and seasonal variations of (b) S4 index and (c) ROTI index as obtained from Global Positioning System receiver at Tirunelveli during the years 2007–2015 and (d) monthly % occurrence of spread *F* at Tirunelveli using CADI ionosonde at Tirunelveli during 2008–2015.

account for strong spread *F* or scintillation occurrences during these two equinoxes. To make this view stronger, we have analyzed the solar flux differences between vernal and autumn equinox during 2007–2015 and corresponding % occurrence differences of spread *F*/L-band scintillations over TIR, which is shown in Table 2. Occurrence statistics of ionosonde spread *F* during 2007 is not available due to its nonavailability. The table shows that % occurrence does not agree well with the solar flux difference between vernal and autumn equinoxes during certain years.

3.2. Characteristics of Spread *F* Over Tirunelveli During 2015

Here we present spread *F* observations over TIR to examine their characteristics and their variability during a moderate solar activity year, 2015. Figures 3a–3c show the temporal and seasonal variations of (a) ESF

Table 2
Solar Flux Differences Between Vernal and Autumn During 2007–2015 and Their Corresponding % Occurrence of Ionosonde Spread F (L-Band Scintillations) Differences Over Tirunelveli

Year	Avg. solar flux (sfu) (vernal)	Avg. solar flux (sfu) (autumn)	Higher solar flux (vernal/autumn)	% occ. of ionosonde spread F(GPS scintillations) (vernal)	% occ. of ionosonde spread F (GPS scintillations) (autumn)	Higher spread *F* (GPS scintillations) (vernal/autumn)
2007	64.975	60.740	Vernal	-- (6.00)	--(1.00)	Vernal
2008	64.330	60.955	Vernal	29.50 (1.50)	50.00 (1.00)	Autumn (Vernal)
2009	62.335	64.225	Autumn	57.40 (2.00)	45.80 (0.00)	Vernal
2010	71.260	73.210	Autumn	84.25 (15.00)	72.00 (11.00)	Vernal
2011	106.430	122.940	Autumn	77.15 (20.00)	85.00 (23.50)	Autumn
2012	102.895	111.105	Autumn	77.00(19.50)	83.70 (20.50)	Autumn
2013	106.230	106.120	Vernal	88.40 (26.50)	56.25 (19.00)	Vernal
2014	132.245	135.910	Autumn	100.00 (30.00)	87.00 (16.00)	Vernal
2015	114.985	92.850	Vernal	83.50 (23.50)	55.63 (11.00)	Vernal

Note. Bracketed values are for L-band scintillations.

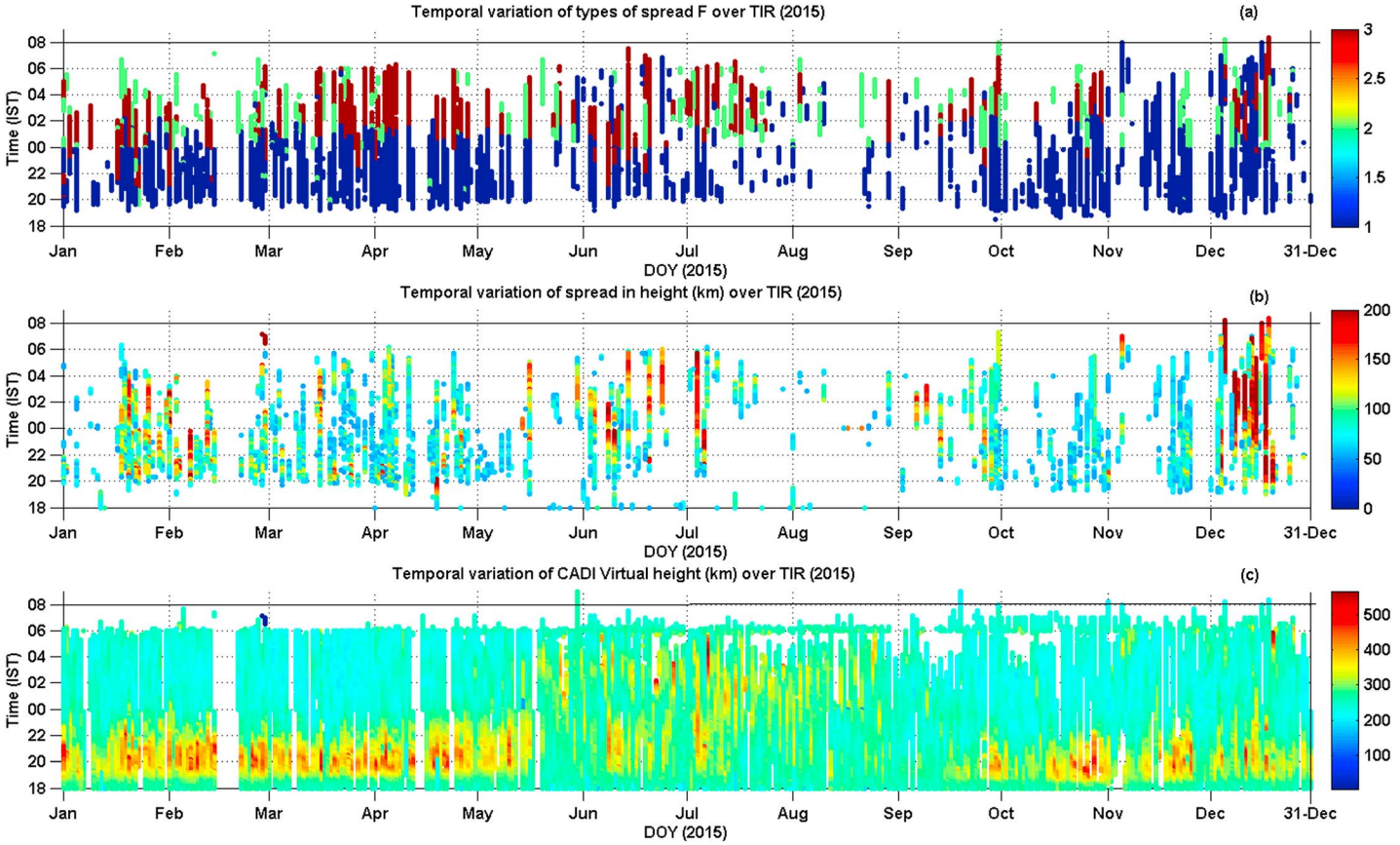

Figure 3. The temporal and seasonal variations of (a) equatorial spread *F* irregularities, (b) spread in the range (km), and (c) virtual height (km) over Tirunelveli respectively for the year 2015.

irregularities, (b) spread in the range, and (c) virtual height (km) over TIR respectively during the year 2015. While *x* axis shows the day of the year, *y* axis shows the time (IST). The color bar in Figure 3a indicates the different classification of spread *F* irregularities, namely "Range," "Frequency," and "Mixed" spread *F* as per the display of the ionograms, which are represented as "1," "2," and "3," respectively. Similarly, the color bar in Figure 3b shows the range spread in kilometers, while *F* layer virtual height, which is representative of prereversal enhancement (PRE), is shown in Figure 3c. The blank spaces indicate data gap due to instrument failure. Figures 4a and 4b show the monthly % occurrence of (a) range spread *F* and (b) frequency and mixed spread *F*. The observations suggest that mostly we observe range spread *F* during the spread *F* onset time, which later becomes frequency and mixed spread *F*. During summer season, it can be seen that spread *F* not only start appearing late as compared to other seasons but also they are short lived. The range spread in Figure 3b indicates that their spreading is large during spread *F* initiation and the spread seems to be strong in the postmidnight during summer season. Interestingly, we observe large spread during December in the winter season. Variations of postsunset height as seen in Figure 3c suggest that they are dominant during January-February, March-April, September-October, and December periods. However, during May-August period, the PRE seems to have mixed time variations where it enhances in the postsunset hours on some events and during postmidnight hours on other events. The late spread *F* occurrence during summer season also indicates that they are of different type. These observations can be seen clearly in the Figure 4. During the year 2015, the mean monthly solar flux is varied in the range of 110–120 sfu during first half of the year. But, the solar flux drastically reduced to ~100 sfu during July and August. The solar flux afterward varied at 90–100 sfu range with minimum of 92 sfu being recorded at autumn equinox. So the results suggest that the occurrence of ESF irregularities during equinoxes at TIR is behaved as per the solar flux difference with maximum being observed in vernal equinox, while in summer they behaved differently. However, the second largest number of ESF events is recorded during winter after vernal equinox during 2015.

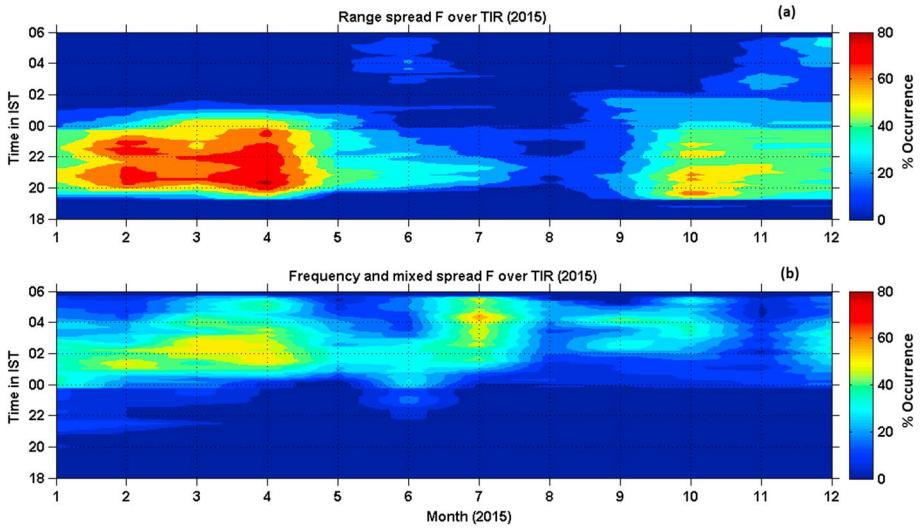

Figure 4. The monthly % occurrence of (a) range and (b) frequency and mixed spread *F* during 2015.

3.3. Simultaneous Occurrence of Spread *F* at Tirunelveli/Hyderabad/Allahabad During 2015

In order to study the latitudinal variation of spread *F* observations, we analyzed ionosonde data from Hyderabad and Allahabad stations in addition to TIR station. Figures 5a–5c show the monthly percentage of spread *F* occurrence over TIR, Hyderabad, and Allahabad, respectively, during the year 2015. From the observations, it is evident that the ESF is dominant over TIR followed by Hyderabad in the equinoxes and winter season; however, no such spread *F* is seen in Allahabad during the same period. Also, the occurrence map at TIR and Hyderabad suggests that vernal equinox is more dominant than that of other seasons, which is also matching with GPS L-band scintillations and ROTI occurrence maps. Even though their scale sizes are different, they mostly follow the same trend. Now we have to understand the reasons for disappearance of spread *F* during equinoxes at Allahabad. There could be two reasons for their disappearance over Allahabad. One of the reasons could be spread *F* may not reach Allahabad to be seen in ionograms. It is because the irregularities at equator need to rise to the Apex altitude of 800–1,000 km to be visible in Allahabad. The other reason could be that we noticed many blank ionograms due to low sensitivity during the postsunset period during 2015, and hence, we are not able to see spread *F* over Allahabad during equinox and winter seasons. However, during summer season, we have seen many days having strong spread *F* in the postmidnight sector

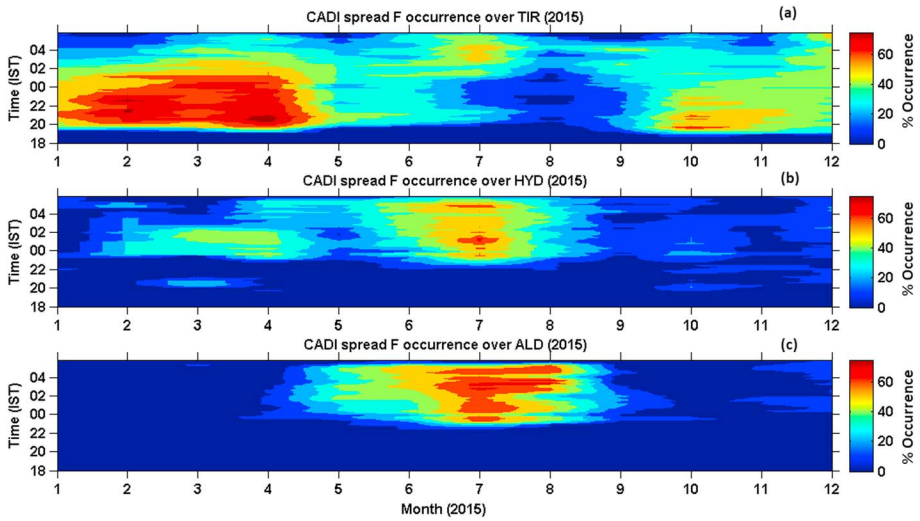

Figure 5. The monthly percentage of spread *F* occurrence over (a) Tirunelveli (TIR), (b) Hyderabad (HYD), and (c) Allahabad (ALD), respectively, during the year 2015.

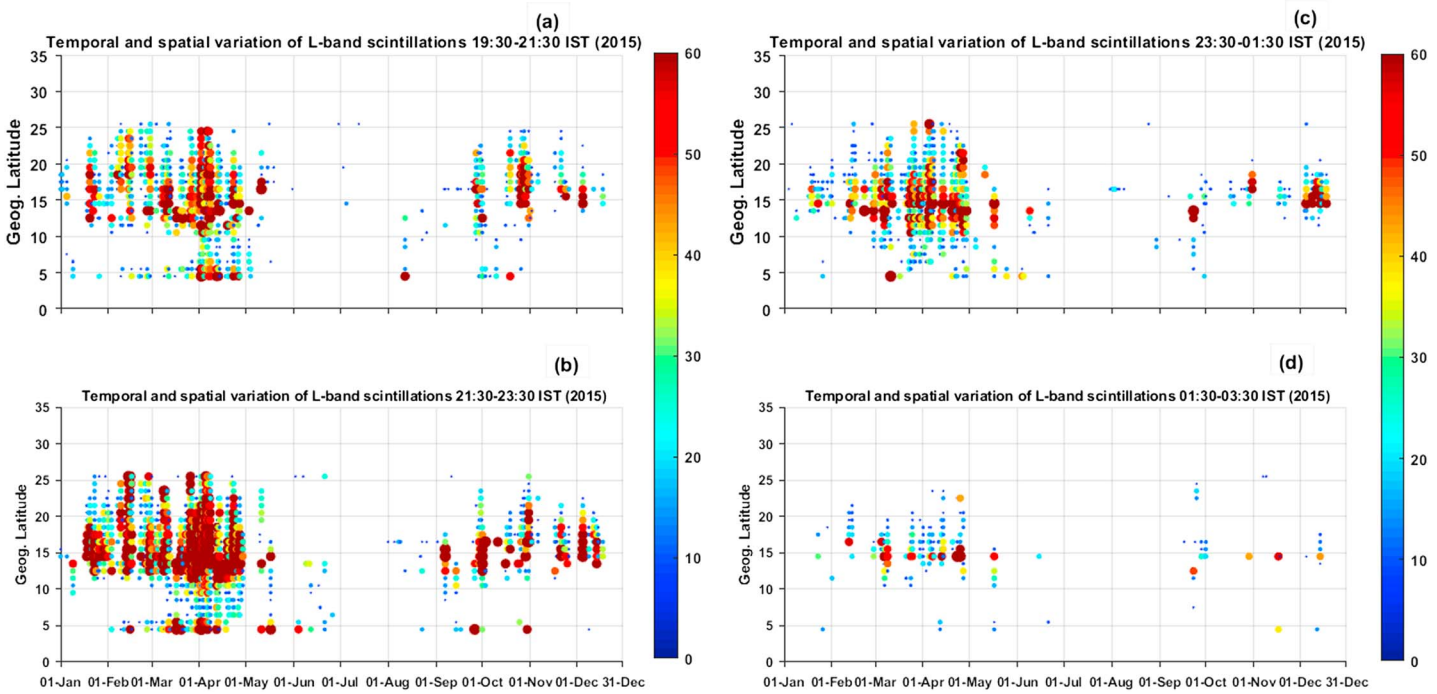

Figure 6. The scatter plot of % occurrence of latitudinal and seasonal variation of Global Positioning System L-band scintillations during (a) 19:30–21:30 IST, (b) 21:30–23:30 IST, (c) 23:30–01:30 IST and (d) 01:30–03:30 IST) after applying elevation threshold of 30°.

over Allahabad. These observations are reflected in spread *F* occurrence in Allahabad station. Further, the observations reveal that percentage of spread *F* occurrence over Allahabad is stronger followed by Hyderabad and TIR station during summer. One interesting aspect that can be noticed from this figure is that Allahabad spread *F* starts at ~22:00–23:00 IST followed by Hyderabad, which is seen at 23:00–24:00 IST. But TIR spread *F* is usually seen after spread *F* is seen at Allahabad/Hyderabad in the postmidnight period. Accordingly, there is a delay in spread *F* onset time as one goes from Allahabad to TIR during summer season, which is prominent in the figure. This observation is in contrast to the spread *F* during equinox and winter seasons.

3.4. Latitudinal Variation of GPS TEC Gradients and L-Band Scintillations During 2015

Here we investigate the characteristics of GPS TEC gradients and L-band scintillations obtained from the network of GPS/GNSS receiver stations, namely, TIR, Mumbai, and Nagpur. Figures 6a–6d show the latitudinal and seasonal variation of GPS L-band scintillations as calculated in terms of percentage of occurrence after combining all the above stations' data and after applying elevation threshold of 30° during (a) 19:30–21:30 IST and (b) 21:30–23:30 IST, (c) 21:30–01:30 IST and (d) 01:30–03:30 IST for the year 2015. The percentage occurrence is calculated for every day using the threshold of S4 index greater than 0.2 for a given time window of 2-hr interval at each 1° latitude from 04–36°N. The ratio between the number of events with S4 $>$ 0.2 to total number of events at a given time period for a given Ionospheric Pierce Point (IPP) latitude will provide % occurrence for a given day and given latitude. Here *x* axis shows the day of the year, *y* axis shows the latitude of IPP. While plotting the scatter plot, the scatter size is linearly increased as per the occurrence strength of S4 index. From the figure, it can be seen that larger scatter sizes near the anomaly crest than at equatorial locations. The observations also suggest that while L-band scintillations are very strong during vernal equinox, they are moderate during autumn equinox and winter seasons. The latitudinal extent also seems to be wider during vernal equinox. However, L-band scintillations are very weak/absent during summer season as can be seen in Figure 6. Figures 7a–7d show the scatter plot of latitudinal and seasonal variations of mean TEC for every 2-hr time interval, namely, (a) 19:30–21:30 IST and (b) 21:30–23:30 IST, (c) 21:30–01:30 IST and (d) 01:30–03:30 IST quite similar to that of the Figure 5 during the year 2015. While plotting the scatter plot, the marker size is linearly increased as per the strength of TEC. This is in a way represents the TEC gradients. It can

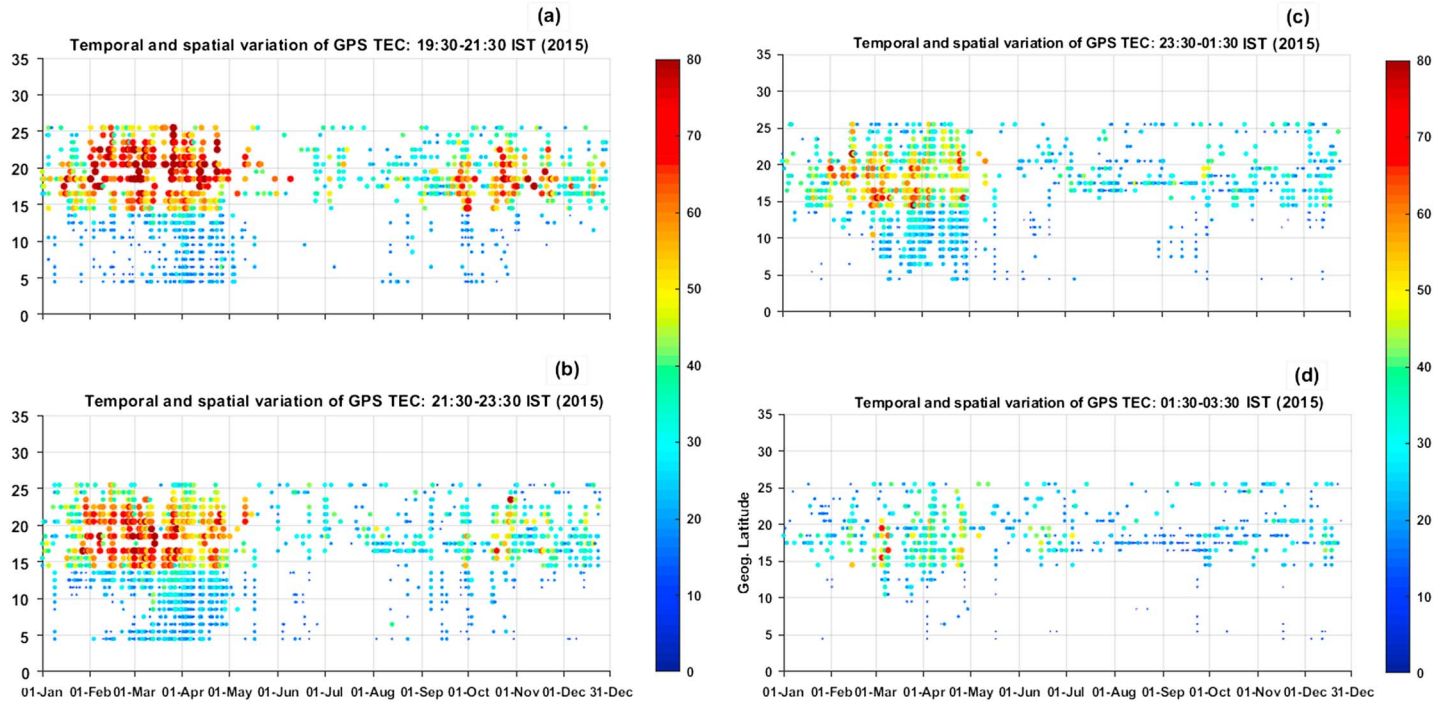

Figure 7. The scatter plot of latitudinal and seasonal variation of mean TEC at (a) 19:30–2130, (b) 21:30–23:30, (c) 23:30–01:30, and (d) 01:30–03:30 IST during the year 2015. The elevation threshold of 30° is used while generating these plots.

be seen that larger TEC and TEC gradients exist near EIA crest region during vernal equinox than observed for other seasons. It is possible that such large TEC and its sharp gradients may be responsible for such strong L-band scintillations as seen during vernal equinox as compared to other seasons (see Figure 6). Also, the observations show the reduction of TEC strength and its gradients slowly moved to lower latitudes with time from crest regions.

3.5. Correlation Between PRE and Strength of S4 Index Over Mumbai/Nagpur

It is usually believed that the postsunset height is very important for the spread *F* occurrence. Accordingly, the scintillation strength also can vary depending upon the postsunset height rise. Also, it is seen in the earlier figures that the GPS L band scintillations are very strong at EIA crest region due to large density gradients, but they are very weak over the equator mainly due to lesser density gradients. Correlation analysis is performed to examine the relationship between the postsunset height rise and the scintillation strength at EIA crest zone and equator. Though these relations are known to be existing qualitatively, no attempt has been made to relate them quantitatively, which is examined here in these plots. These correlations are mostly related to equinox and winter seasons, since GPS scintillations are mostly seen during these two seasons. Figures 8a–8d show the correlation of (a) maximum S4 index at TIR versus maximum S4 index over Mumbai, (b) maximum S4 index at Mumbai versus PRE height (km) at TIR, (c) maximum S4 index over TIR versus maximum S4 index at Nagpur, and (d) maximum S4 index at Nagpur versus PRE height (km) at TIR, respectively, during the year 2015. The correlation coefficients along with number of data points are also shown on top of each plot. Also shown is the least squares linear correlation fit in blue color. The correlation plots suggest that there seem to have some relationship between maximum S4 index over Mumbai (Nagpur) and maximum S4 index over TIR though there is a large deviation (correlation coefficients [*R*] are 0.48 and 0.54, respectively, for Figures 8a and 8c). Similarly, the correlation plots suggest that the maximum S4 index over Mumbai (Nagpur) is linearly correlated with PRE height over TIR (correlation coefficients [*R*] are 0.32 and 0.47, respectively, for Figures 8b and 8d). The S4 index at Nagpur has better correlation with PRE strength and S4 strength at TIR than for Mumbai. From these plots, it is suggested that the PRE height and the maximum strength of S4 index at anomaly crest region are seems to be related to each other. However, care must be taken while interpreting these results as the data set that is used here is not exhaustive.

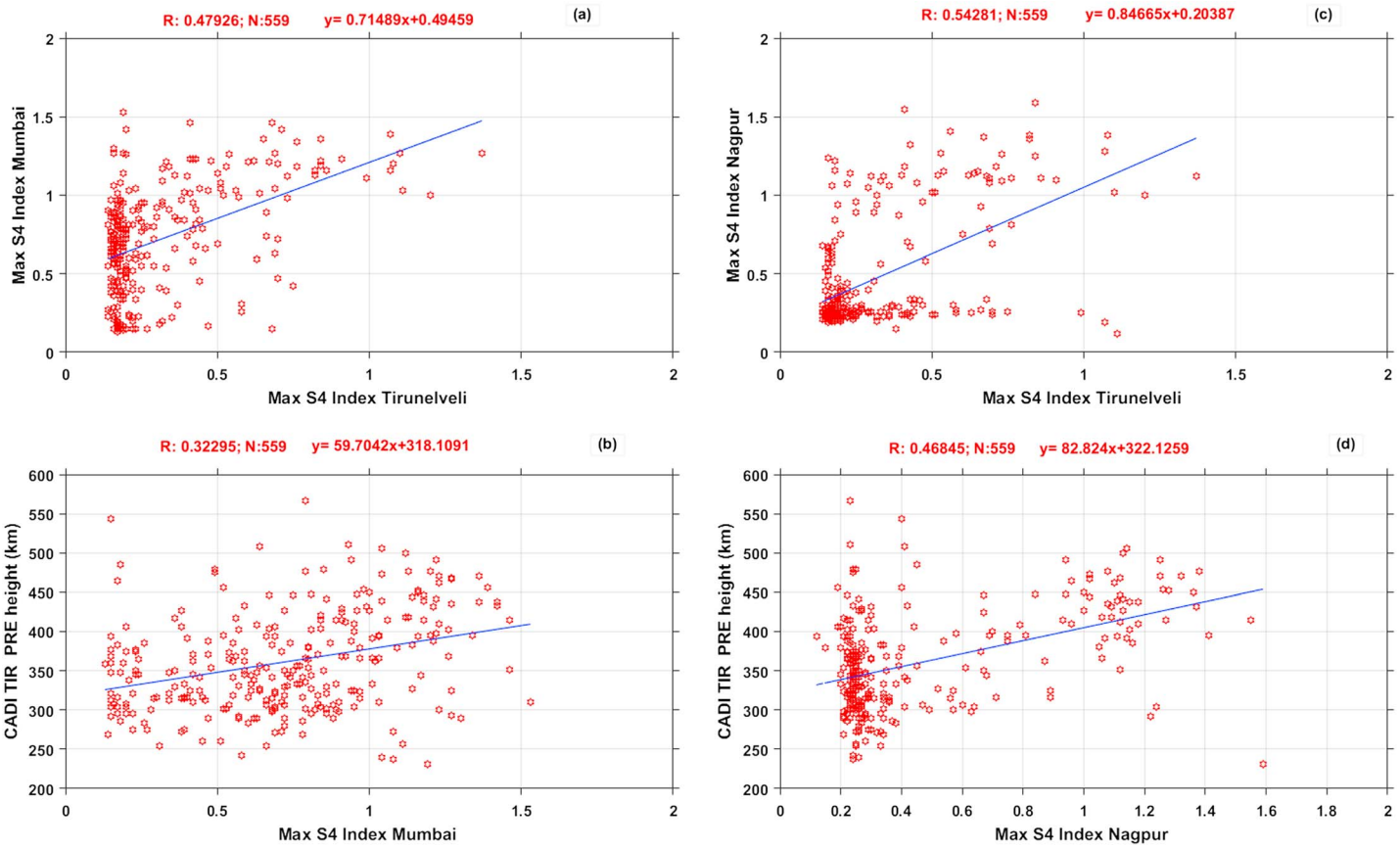

Figure 8. The correlation of (a) max. S4 index over Tirunelveli versus max. S4 index at Mumbai, (b) max. S4 index at Mumbai versus PRE height (km), (c) max. S4 index over Tirunelveli versus max. S4 index at Nagpur, and (d) max. S4 index at Nagpur versus PRE height (km), respectively, for the year, 2015.

3.6. Typical Example of Traveling Ionospheric Disturbances During Summer

We came to know earlier from Figure 5 that spread *F* is observed initially at Allahabad followed by Hyderabad and TIR, respectively, in the summer season, which is quite opposite to other seasons. Accordingly, we examined the *F* layer movements in the meridional direction during summer season to identify the reasons behind their peculiar characteristics. Now we present a typical example of *F* layer variations in terms of isoheight (fixed height) variations during 4 July 2015 simultaneously over Allahabad, Hyderabad, and TIR, where *F* layer is seen to have undergone density undulations. This is shown in Figures 9a–9c. Here different colors indicate density undulations of the different isoheights between 250 and 350 km at every ~20 km altitude. Here the isoheight refers to the frequency variations at a fixed altitude. From top to bottom, the figure represents temporal variation of isoheights at (a) TIR, (b) Hyderabad, and (c) Allahabad, respectively. Such type of analysis is usually done to study the wave structures such as traveling ionospheric disturbances (TIDs) and gravity waves in the ionosphere (e.g., Taori et al., 2015). The red "asterisks" in each subplot indicate "spread *F*." These observations also indicate that the temporal variations of these density fluctuations appear to propagate from Allahabad station to further lower latitudes apparently quite similar to the observations of medium-scale traveling ionospheric disturbances (MSTIDs) as reported frequently for the midlatitudes (e.g., Miller et al., 2009). Based on C/NOFS satellite observations, Huang (2016) have also suggested that TID-like disturbances are observed in the lower latitudes. Similar type of observations is reported in the optical airglow observations over the Indian region (closer to equator) recently (e.g., Taori et al., 2015).

3.7. Correlations of PRE and S4 Index With Various Parameters During 2011–2015

In this section, we present various ionospheric correlations obtained using a large data set, namely, during 2011–2015. Here we use CADI ionosonde PRE height data along with L-band scintillations obtained from a

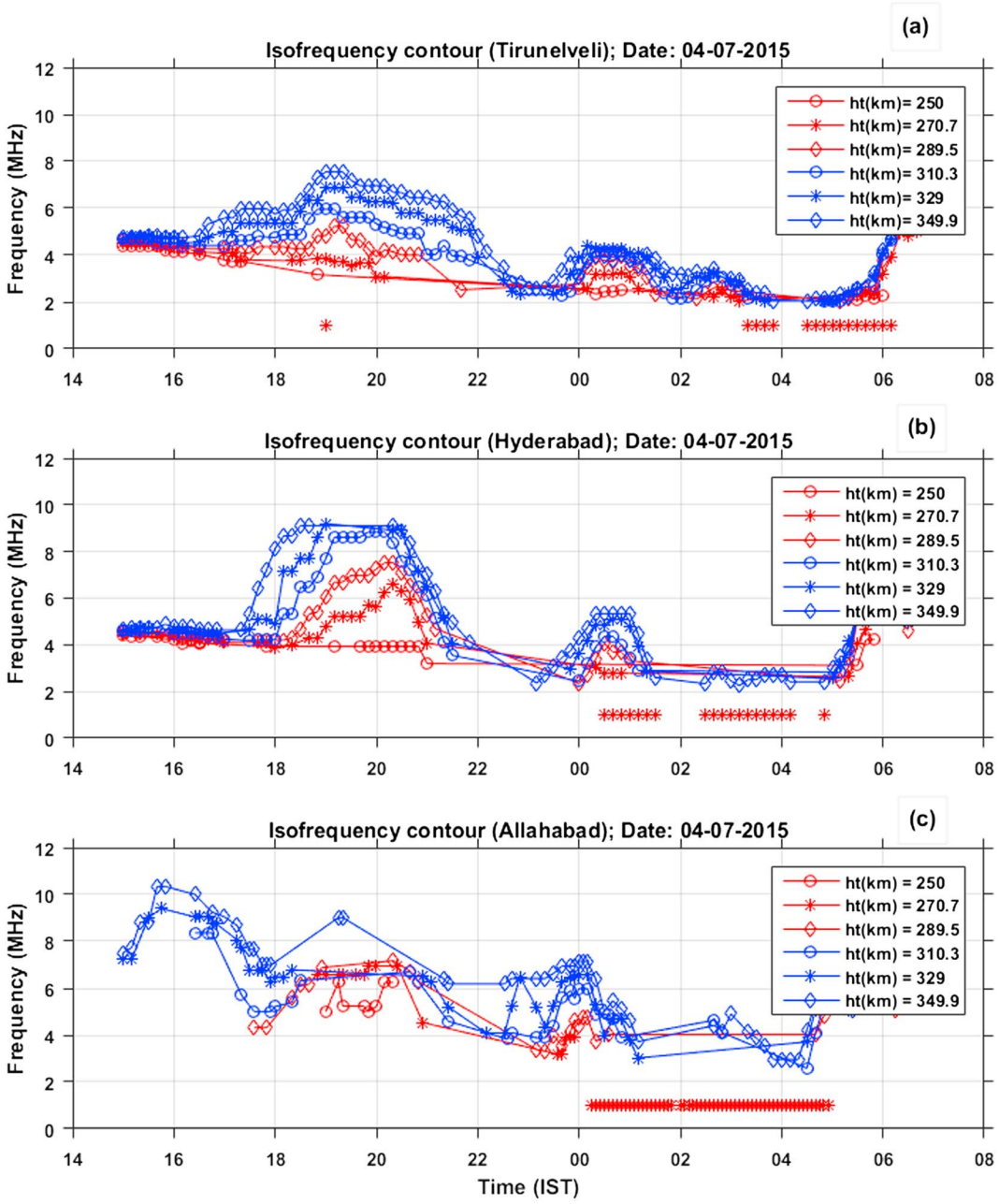

Figure 9. The temporal variation of frequency (density) undulations of ionosonde *F* region observations, which is at fixed (virtual heights) altitudes (ht [km]: 250, 270, 290, 310, 330, and 250) over (a) Tirunelveli, (b) Hyderabad, and (c) Allahabad on 4 July 2015. The red "asterisks" in each subplots indicate "spread *F*."

collocated GPS receiver at TIR. We also use EEJ strength data in this study. Though some studies were done earlier, we use a large data set to provide statistically meaningful information in this exercise. It may be noted that we use daily integrated (int.) EEJ strength data during evening hours between 17:00 and 19:00 IST to correlate it to the PRE height, which is believed to be related to spread *F* occurrence. The daily sum of Kp index between 17:30 and 20:30 IST (between 12 UT and 15 UT) is used as a proxy for geomagnetic activity. Figures 10a–10f show the correlation of (a) int. EEJ strength versus PRE height (km), (b) PRE height (km) versus solar flux, (c) maximum S4 index (TIR) versus solar flux, (d) maximum S4 index (TIR) versus PRE height (km), (e) Kp index versus PRE height (km), and (f) Kp index versus maximum S4 index (TIR). Here while the blue color indicates nonscintillation event, the red color indicates scintillation event based on the threshold of S4 index of 0.25. The correlation coefficients as obtained using least squares fit are given

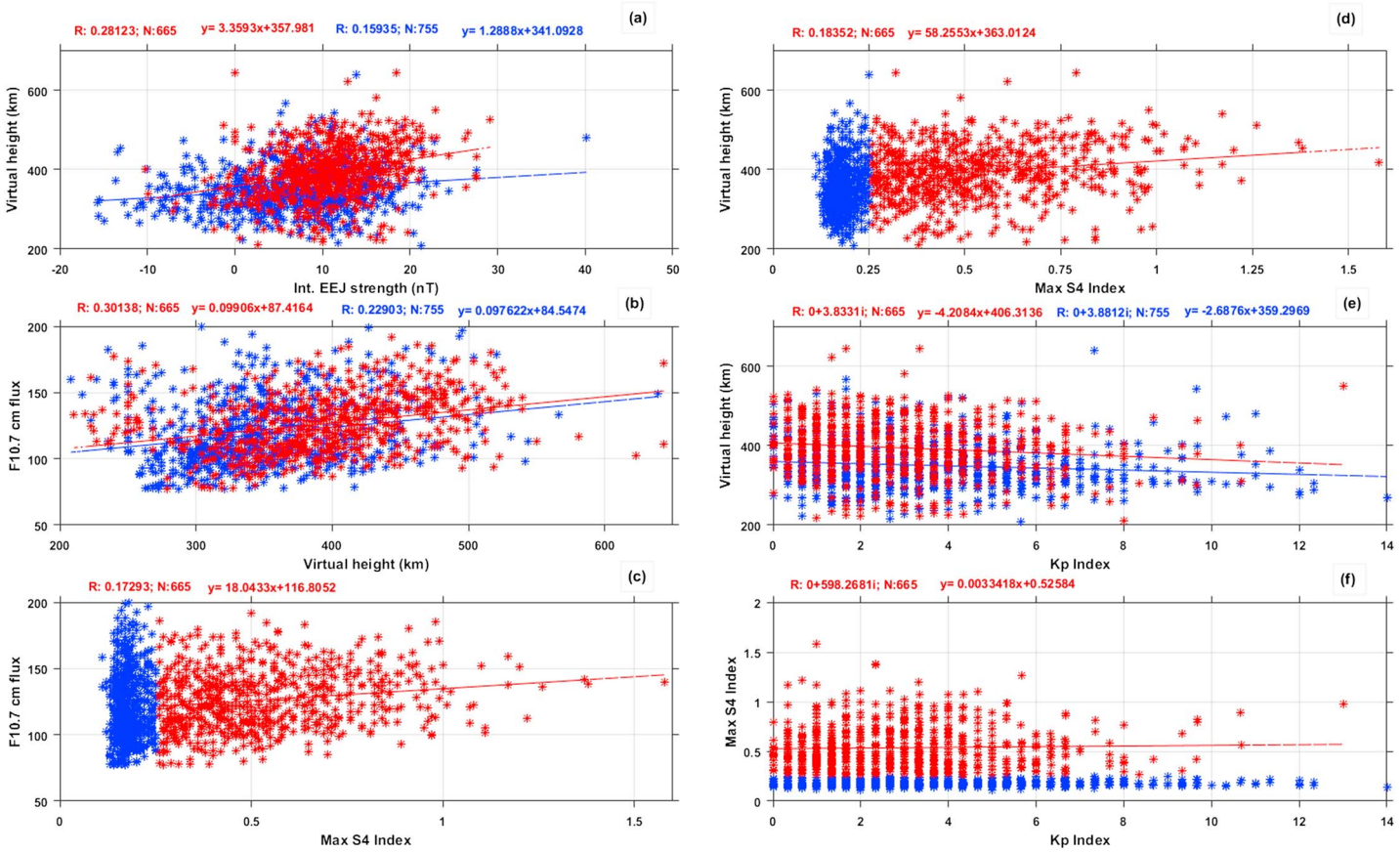

Figure 10. The correlation of (a) int. EEJ strength versus PRE height (km), (b) PRE height (km) versus solar flux, (c) max. S4 index versus solar flux, (d) max. S4 index versus PRE height (km), (e) Kp index versus PRE height (km), and (f) Kp index versus max. S4 index.

on the top of each plot. We have drawn two fitting lines (blue for nonscintillations and red for scintillations) for plots (a), (b), and (e) to show the differences between scintillations versus nonscintillation days. It is noticed that correlation improved for the days when scintillations were present than for the days when scintillations were absent. From the plots, it is evident that as PRE height increases, S4 index strength seems to increase, and as solar flux increases, S4 index seems to increase. But poor correlation coefficients were seen in the plots mainly due to large scatter in the data. Similarly, as int. EEJ strength increases, PRE height seems to increase. However, when Kp index increases, PRE height showed negative slopes with complex correlations suggesting that spread *F* irregularities may be suppressed or reduced during geomagnetic activity in the premidnight sector. However, S4 strength is not showing any correlation with Kp index. Though, this analogy can be drawn from this analysis, but it does not give clear indication. This suggests that the problem is complex and many factors seem to play simultaneously.

4. Discussions

While stronger and longer duration ESF irregularities are found to occur in the postsunset during equinoxes and winter solstice, they are weaker in strength and shorter in duration during summer season in the postmidnight sector. The PRE height also seems to be very strong during equinoxes followed by winter and summer, respectively. Further, the results suggest that the irregularities during equinoxes and winter are seen with diminishing strength right from the equator to the low latitudes. However, interestingly, our results indicate that the plasma irregularities as seen in the postmidnight sector during summer season are found to be stronger and much earlier at Allahabad, a lower latitudinal station followed by Hyderabad and TIR (equatorial station). Also, the observations suggest that the spread *F* during summer is noticed only in the ionosondes, while it is seen in both the ionosondes and GPS receivers during equinox and winter seasons. It is understood

that due to low background electron density in the postmidnight sector, the L-band scintillations that arise from the irregularities of 400 m scale size are not observed frequently during postmidnight sector in the summer season. Also, it depends on the scale size of the irregularities that are present in the medium to cause scintillations. Since L-band scintillations are mostly caused by the irregularities of intermediate scale size, these scale size of irregularities may not be present in the postmidnight sector to cause scintillations (as smaller scale size irregularities disappear sooner than kilometer-scale size irregularities), which is contrary to other scale sizes (e.g., Basu et al., 1978; Sripathi et al., 2008). The results further suggest that while irregularities during equinox and winter seasons are mostly controlled by electric field-driven processes as irregularities are first observed at equator and then at other latitudes, the irregularities as seen in the postmidnight sector at the equator and other low latitudes during summer season may be of midlatitude origin as they first observed at low latitudes and then at equator. Our results also reiterate that there exists a strong equinoctial asymmetry in the occurrence of plasma irregularities and scintillations where vernal (autumn) equinox showed strong (weak/moderate) occurrence of plasma irregularities.

The correlation analysis performed using the larger data set of PRE height from ionosonde and GPS L-band scintillations for the years 2011–2015 (5 years) over TIR suggests certain relations between plasma irregularities and scintillations with solar flux, integrated (int.) EEJ strength and Kp index. The correlations suggest that while PRE height (in the evening) and solar flux are correlated to produce strong scintillations/plasma irregularities, they are negatively correlated to Kp index. In addition, the correlation plots suggest that there is a linear relationship between the maximum strengths of S4 index over Mumbai (Nagpur) and TIR. Similarly, the results suggest that the maximum strength of S4 index over Mumbai (Nagpur) is linearly correlated with PRE height over TIR, with a few deviations. The dependence of plasma irregularities on the $E \times B$ drift and Kp index during different seasons is investigated by Whalen (2002) and suggested that the plasma irregularities are linearly dependent (inversely) on Kp index during equinoxes and winter solstice; however, they are independent of Kp index during summer. Tulasi Ram et al. (2006) have extended the same study to the Indian sector to understand the combined effects of the daytime int. EEJ strength and the Kp index on the PRE height, which are believed to be the controlling factors of ESF irregularities. While their results do suggest that linear relationship exists between PRE height and daytime int. EEJ strength, Uemoto et al. (2010) later suggested that rather than integrating entire daytime EEJ strength, integration of EEJ strength around sunset seems to play an important role in the PRE development as it causes conductivity gradients of the *E* region at the sunset. Our observations of PRE decrease with increase of Kp indicate that the ESF irregularities could be suppressed due to penetration of westward electric fields to the existing eastward PRE electric fields resulting in decrease of PRE. These observations are supporting their findings. However, our observations do not show good correlation with evening time int. EEJ strength, which is in contrast to the results of Uemoto et al. (2010). While the correlations of ESF irregularities with PRE height, int. EEJ strength, solar flux, and Kp index are studied earlier, here we present them using a larger data set and also based on L-band scintillations.

Equinoctial asymmetry as seen here is quite frequent over Indian sector. One of the probable factors for the equinoctial asymmetry is the asymmetric distribution of solar fluxes. The probable factors that depend very much on solar flux are PRE height, thermospheric winds, collision frequencies, and plasma density. Accordingly, they may play an important role in this asymmetry. It is suggested that one of the factors for equinoctial asymmetry could be due to asymmetric thermospheric meridional winds during these two equinoxes (Maruyama et al., 2009). Using the GPS L-band scintillations during 2004–2005, Sripathi et al. (2011) suggested that asymmetry in the occurrence of plasma irregularities and their latitudinal extent for these two equinoxes could be due to asymmetric PRE height and asymmetric distribution of ionization crests. Further, they have shown the existence of asymmetric (symmetric) crests of peak electron density (N_mF_2) about the equator during the autumn (vernal) equinox even though the solar flux differences between the vernal and autumn equinox periods are insignificant. Nishioka et al. (2008) suggested that the equinoctial asymmetry in the occurrence of plasma bubbles could be due to the asymmetric distribution of integrated conductivities. Our observations of higher PRE height during 2015 suggest that these enhanced PRE drifts could be responsible for higher number of scintillations or ESF irregularities during the vernal equinox when compared with the autumn equinox. The same observations exist for a few years and vice versa for the other few years as noticed in the earlier section. The fewer number of scintillations or ESF are seen during the (vernal) autumn equinox where PRE drifts are small suggesting that the scintillations could have been suppressed by lower PRE drifts. Such lower PRE drifts during (vernal) autumn equinox are bound to be affected by higher

collisions and higher recombination that can affect the development of spread *F* at lower heights. On the other hand, Ren et al. (2011) suggested that the equinoctial asymmetry could be due to the manifestation of annual variation of plasma densities and meridional/zonal winds. Our observations suggest that the equinoctial asymmetry consistently persists during the observation period presented here, but it varies closely with the PRE drifts and solar flux on many occasions. For certain years, though the solar flux is equal during equinoxes, the PRE drifts and spread *F* occurrence are different (see Table 2). So it is possible that in addition to solar flux, there are other factors such as gravity waves, tides, and winds that may play significant role in this equinoctial asymmetry.

Now we discuss the possible causes for the occurrence of postmidnight sector plasma irregularities during summer. Fewer observations were available earlier to study the characteristics of spread *F* in the summer season. These kind of skewed observations are mostly due to nonexistence or weaker strength of plasma irregularities in the postmidnight sector. Postmidnight sector plasma irregularities are usually believed to be part of prolonged premidnight sector irregularities. These irregularities are believed to be not as turbulent as that of postsunset sector irregularities. Earlier, Sastri et al. (1997) and Chandra and Rastogi (1972) and Subbarao and Murthy (1994) have carried out some studies over Indian region during the summer season. Their results suggest that the summer spread *F* is usually inversely proportional to solar flux. Here we too observe frequent postmidnight spread *F* occurrence during summer season in the low solar activity years. Patra et al. (2009) investigated the very high frequency radar echoes in the postmidnight sector at Gadanki during summer season in the low solar activity years and suggested that these irregularities could be generated through the gradient drift assisted RT instability. Since there is no evidence that these irregularities could be drifted-in from other longitudes where they might have generated in the postsunset sector, they suggested that it could be driven by local sources. Sastri (1999) investigated the variability of summer postmidnight spread *F* over Kodaikanal using ionosonde and suggested that other factors such as thermospheric meridional winds and vertical winds may be controlling the RT instability on individual nights in addition to PRE. Since equatorial midnight temperature maximum is strongest in summer, it is believed that the day-to-day variability of midnight temperature maximum could induce corresponding variability in the spread *F* occurrence in the postmidnight sector. When ionosonde height rise is not seen prior to the spread *F* occurrence during summer on some events, it is suggested that the onset of postmidnight spread *F* might have not generated locally but they are drifted-in patches that formed elsewhere either east or west of the ionosonde station. Niranjan et al. (2003) have also concluded with same reasoning for summer spread *F* during postmidnight. We do see mixed variations in our observations of height rise of the *F* layer in the postmidnight sector suggesting that some of the spread *F* events may be generated immediately after the height rise but some of the spread *F* events did not relate to height rise but they could be either drifted-in or generated by other sources.

Since Es layers are very common and strong during summer season, Tsunoda (2007) suggested that polarization electric fields generated in the Es layers may map to the *F* region and can cause the Perkins type of instability in the midlatitudes during summer season. Accordingly, some experimental evidences for the relationship between the midlatitude structures and the development of postmidnight ESF during geomagnetic quiet conditions are investigated by Miller et al. (2009). They suggested that their results are in agreement with the hypothesis of Tsunoda (2007). In the postsunset equatorial ionosphere, the plasma irregularities are generated by zonal neutral winds and evening plasma vertex, which are necessary to initiate the RT instability that produces depletions. However, since the differential motion between the zonal neutral winds and zonal plasma drift is small in postmidnight sector, the above mechanism may be ineffective. Thus, they suggested that postmidnight spread *F* at solar minimum cannot be dominated by this mechanism. Instead they suggested that the generation of polarization electric fields (E_p) is possible with the passage of the MSTIDs that could provide the necessary seed perturbation required for the generation of plasma irregularities during postmidnight sector. As described by Cosgrove and Tsunoda (2002), coupling of the altitude modulated Es layers in the midlatitude *E* region in the ionosphere can map to the base of the *F* region and can generate the polarization electric field structures having similar characteristics of MSTIDs. Based on the results presented here, we believe that some of our observations during summer season may not be of equatorial type but they may provide some evidences for MSTID-type mechanism to be operating in the equatorial ionosphere over Indian sector mostly during summer season. But clearly these postmidnight spread *F* irregularities are not visible in the L-band scintillations.

The first observation of MSTIDs, very close to the equator, comes from a narrow field optical imaging system in Chile, South America, though, previously, MSTIDs were not thought to be present close to the equator (Makela et al., 2010). They suggested that these MSTIDs are propagating westward and toward the equator from northwest to southeast in the northern hemisphere and southwest to northeast in the southern hemisphere. Since Allahabad is located at the east of TIR, our observations of spread *F* first at Allahabad followed by TIR do suggest westward propagation. However, we do not have proper data to examine their orientations. On the other hand, Otsuka et al. (2012) have investigated the radar echoes during low solar activity period over Kototabung, Indonesia, and suggested that most of the plasma irregularities were drifting toward west, which cannot be accounted for equatorial plasma bubbles. Hence, they suggested that postmidnight irregularities as seen in their observations could be associated with MSTIDs. C/NOFS satellite observations also show more plasma density irregularities during postmidnight than in the postsunset sector in the low solar activity period (Dao et al., 2011). It is also suggested that the spread *F* occurrence during June solstices, in the low solar activity, over Cachoeira Paulista, which is in the southern crest of the EIA, is not related to the equatorial type irregularities but could be related to TIDs of midlatitude origin (Candido et al., 2011). Characteristics of postmidnight sector irregularities over the Equatorial Atmospheric Radar (EAR) located in Indonesia suggest that they are of two types where one is associated with upwelling plumes, which are not dead bubbles, and other is like MSTID-like structures that show similarities to midlatitude irregularities (Yokoyama et al., 2011, 2011). These irregularities propagate westward as opposed to the regular postsunset sector ESF irregularities. Background zonal drift velocities as measured by C/NOFS satellite also suggest their westward propagation. Accordingly, the morphological feature of spread *F* in the postmidnight sector during summer solstice in the solar minimum is significantly different from that of the postsunset irregularities. They suggested that topside ionosphere above the magnetic equator that couples with the low-latitude *F* region may be controlled by midlatitude-type dynamo system. Our ionosonde observations of range/frequency spread *F* during summer also suggest that there could be two types of spread *F* in TIR. When postsunset spread *F* is noticed, it is seen as range spread *F*. However, when spread *F* is observed in the postmidnight sector, we observe mostly frequency and mixed type spread *F*. Since EAR is very close to the Indian longitude, our observations of similar characteristics of summer spread *F* do suggest that they are different from regular postsunset sector spread *F* and follows more of EAR characteristics. To identify the source of the seed perturbation to generate the spread *F* irregularities, radio and optical observations are investigated over Indian region (Taori et al., 2015). They noticed that while there are no upward propagating waves recorded in the MLT altitude, their observations at low latitudes showed signatures of tilted east-west wave structures propagating toward equator, which they attributed to MSTIDs. Our observations presented here do suggest that some of the irregularities occur in the postmidnight sector in the summer may be triggered by such nonequatorial processes. Also, our observations of density undulations as shown in Figures 9a–9c suggest that ionization patches were moving from Allahabad to TIR, which is suggestive of MSTID-type disturbances. Such observations are available in plenty during summer.

Yizengaw et al. (2013) suggested that large occurrence of sporadic *E* (Es) in the June solstice at low latitudes could be one of the sources of eastward electric field that led to the formation of plasma bubbles or irregularities during postmidnight sector in the African longitude. They also said that postmidnight plasma bubbles and scintillations are distinctly different during summer and these structures are not continuation of plasma bubbles in the postsunset sector. Analysis of ionosonde observations from Trivandrum and Ahmedabad do suggest that MSTID-type disturbances could be responsible for off-vertical reflections during summer season where PRE is believed to be very low (Rastogi & Chandra, 2015). The observations of nighttime Es layers over Allahabad during low solar activity period in the summer do suggest that Es layers are very much common during summer than other seasons over Allahabad (Tiwari et al., 2012). Accordingly, our observations of strong spread *F* first over Allahabad followed by Hyderabad and TIR during summer suggest that strong Es layers during summer at low latitude might generate polarization electric fields and could map to the base of the *F* region as suggested by Cosgrove and Tsunoda (2002). While this appears to be plausible scenario, still further research is needed to conclude their origin.

5. Summary

We presented characteristics of equatorial and low-latitude plasma irregularities as studied using a meridional chain of ionosondes and GPS receivers covering equator to beyond crest zone over Indian region during a

moderate solar flux year 2015. We also studied the seasonal and solar flux dependence of spread *F* and scintillations using ionosonde and GPS scintillations at TIR with larger data set.

The following are the important results:

1. The observations suggest that while stronger and longer duration ESF irregularities are observed in the postsunset sector during equinoxes and winter solstice, they are weaker and shorter in the postmidnight sector during summer.
2. Further, our results suggest that while the postsunset sector irregularities diminish its strength from the equator to low latitudes during equinoxes and winter, the postmidnight irregularities as seen during summer are found to be stronger and earlier at low latitudes followed by their presence at the equator.
3. While spread *F* is seen mostly in the ionosondes during summer, it is seen in both ionosondes and GPS receivers during equinoxes and winter season.
4. The results, further, suggest that while premidnight irregularities that are generated during equinoxes and winter could be generated by equatorial process linked with "RT instability," some of the postmidnight irregularities that are generated during the summer could be associated with nonequatorial processes such as "MSTIDs."
5. Our results also emphasize that there exists an equinoctial asymmetry in the occurrence of plasma irregularities or scintillations wherein autumn equinox showed weak/moderate occurrence of plasma irregularities and vice versa. Mainly, they appear to be associated with variations in the plasma drifts due to variations in the in the solar flux.
6. In addition, the results further suggest that while plasma irregularities/scintillations and PRE are linearly correlated to solar flux, they are inversely related to the geomagnetic strength, Kp index.

Acknowledgments

The research work that is presented here is carried out at IIG (DST), Government of India. The authors also sincerely thank B. Suneel kumar, TIFR Balloon Facility, Hyderabad, for providing ionosonde data from Hyderabad station. We also would like to thank K. Emperumal at EGRL, Tirunelveli, and Prabhakar Tiwari at KSKGRL, Allahabad, for maintaining CADI ionosondes and N. Venkatesh, EGRL, Tirunelveli, and B. Laxman, Nagpur Observatory, for their support in maintaining GNSS receivers at Mumbai and Nagpur. We also thank Keith Groves, Boston College (USA), for providing access to GPS SCINDA receiver data at Tirunelveli. Solar data used here are obtained from http://omniweb.gsfc.nasa.gov/, while geomagnetic index data are obtained from WDC, Kyoto, Japan. The authors would like to thank the anonymous reviewers for their earnest suggestions/comments. All the data sets presented here are with the corresponding author, and the data request may be sent through his e-mail ssripathi.iig@gmail.com.

References

Abdu, M. A. (2001). Outstanding problems in the equatorial ionosphere-thermosphere electrodynamics relevant to spread *F*. *Journal of Atmospheric and Solar - Terrestrial Physics*, *63*(9), 869–884. https://doi.org/10.1016/S1364-6826(00)00201-7

Abdu, M. A., Kherani, E. A., Batista, I. S., De Paula, E. R., Fritts, D. C., & Sobral, J. H. A. (2009). Gravity wave initiation of equatorial spread *F*/plasma bubble irregularities based on observational data from the SpreadFEx campaign. *Annales de Geophysique*, *27*(7), 2607–2622. https://doi.org/10.5194/angeo-27-2607-2009

Abdu, M. A., MacDougall, J. W., Batista, I. S., Sobral, J. H. A., & Jayachandran, P. T. (2003). Equatorial evening pre-reversal electric field enhancement and sporadic *E* layer disruption: A manifestation of *E* and *F* region coupling. *Journal of Geophysical Research*, *108*(A6), 1254. https://doi.org/10.1029/2002JA009285

Basu, S., Basu, S., Aarons, J., McClure, J. P., & Cousins, M. D. (1978). On the coexistence of kilometer- and meter-scale irregularities in the nighttime equatorial *F* region. *Journal of Geophysical Research*, *83*(A9), 4219–4226. https://doi.org/10.1029/JA083iA09p04219

Buhari, S. M., Abdullah, M., Yokoyama, T., Otsuka, Y., Nishioka, M., Hasbi, A. M., et al. (2017). Climatology of successive equatorial plasma bubbles observed by GPS ROTI over Malaysia. *Journal of Geophysical Research: Space Physics*, *122*, 2174–2184. https://doi.org/10.1002/2016JA023202

Burke, W. J., Gentile, L. C., Huang, C. Y., Valladares, C. E., & Su, S. Y. (2004). Longitudinal variability of equatorial plasma bubbles observed by DMSP and ROCSAT-1. *Journal of Geophysical Research*, *109*, A12301. https://doi.org/10.1029/2004JA010583

Candido, C. M. N., Batista, I. S., Becker-Guedes, F., Abdu, M. A., Sobral, J. H. A., & Takahashi, H. (2011). Spread *F* occurrence over a southern anomaly crest location in Brazil during June solstice of solar minimum activity. *Journal of Geophysical Research*, *116*, A06316. https://doi.org/10.1029/2010JA016374

Chandra, H., & Rastogi, R. G. (1972). Equatorial spread-F over a solar cycle. *Annales de Geophysique*, *28*(4), 709–716.

Cosgrove, R. B., & Tsunoda, R. T. (2002). A direction-dependent instability of sporadic-*E* layers in the nighttime midlatitude ionosphere. *Geophysical Research Letters*, *29*(18), 1864. https://doi.org/10.1029/2002GL014669

Dao, E., Kelley, M. C., Roddy, P., Retterer, J., Ballenthin, J. O., de La Beaujardiere, O., & Su, Y.-J. (2011). Longitudinal and seasonal dependence of nighttime equatorial plasma density irregularities during solar minimum detected on the C/NOFS satellite. *Geophysical Research Letters*, *38*, L10104. https://doi.org/10.1029/2011GL047046

Fejer, B. G., & Kelley, M. C. (1980). Ionospheric irregularities. *Reviews of Geophysics and Space Physics*, *18*(2), 401. https://doi.org/10.1029/RG018i002p00401

Gentile, L. C., Burke, W. J., & Rich, F. J. (2006). A climatology of equatorial plasma bubbles from DMSP 1989–2004. *Radio Science*, *41*, RS5S21. https://doi.org/10.1029/2005RS003340

Huang, C., Burke, W., Machuzak, J., Gentile, L., & Sultan, P. (2002). Equatorial plasma bubbles observed by DMSP satellites during a full solar cycle: Toward a global climatology. *Journal of Geophysical Research*, *107*(A12), 1434. https://doi.org/10.1029/2002JA009452

Huang, C.-S. (2016). Plasma drifts and polarization electric fields associated with TID-like disturbances in the low-latitude ionosphere: C/NOFS observations. *Journal of Geophysical Research: Space Physics*, *121*, 1802–1812. https://doi.org/10.1002/2015JA022201

Kelley, M. C., Makela, J. J., de La Beaujardière, O., & Retterer, J. (2011). Convective ionospheric storms: A review, *Reviews of Geophysics*, *49*, RG2003. https://doi.org/10.1029/2010RG000340

Kudeki, E., & Bhattacharyya, S. (1999). Postsunset vortex in equatorial *F*-region plasma drifts and implications for bottomside spread–*F*. *Journal of Geophysical Research*, *104*(A12), 28,163–28,170. https://doi.org/10.1029/1998JA900111

Li, G., Baiqi, N., Libo, L., Weixing, W., Lianhuan, H., Biqiang, Z., et al. (2012). Equinoctial and June solstitial *F*-region irregularities over Sanya. *Indian Journal of Radio and Space Research*, *41*, 184–198.

MacDougall, J. W., Grant, I. F., & Shen, X. (1995). The Canadian Advanced Digital Ionosonde—Design and results, *Ionosonde Network and Stations Rep. UAG. 104*, *pp. 21–27*, *World Data Center for Solar Terrestrial Physics*.

Makela, J. J., Miller, E. S., & Talaat, E. R. (2010). Nighttime medium-scale traveling ionospheric disturbances at low geomagnetic latitudes. *Geophysical Research Letters*, *37*, L24104. https://doi.org/10.1029/2010GL045922

Maruyama, T., Saito, S., Kawamura, M., Nozaki, K., Krall, J., & Huba, J. D. (2009). Equinoctial asymmetry of a low-latitude ionosphere-thermosphere system and equatorial irregularities: Evidence for meridional wind control. *Annales de Geophysique*, *27*(5), 2027–2034. https://doi.org/10.5194/angeo-27-2027-2009

Miller, E. S., Makela, J. J., & Kelley, M. C. (2009). Seeding of equatorial plasma depletions by polarization electric fields from middle latitudes: Experimental evidence. *Geophysical Research Letters*, *36*, L18105. https://doi.org/10.1029/2009GL039695

Niranjan, K., Brahmanandam, P. S., Ramkrishnarao, P., Uma, G., Prasad, D. S. V. V. D., & Ramarao, P. V. S. (2003). Post midnight spread-*F* occurrence over Waltair (17.7°N, 83.3°E) during low and ascending phases of solar activity. *Annales de Geophysique*, *21*(3), 745–750. https://doi.org/10.5194/angeo-21-745-2003

Nishioka, M., Saito, A., & Tsugawa, T. (2008). Occurrence characteristics of plasma bubble derived from global ground-based GPS receiver networks. *Journal of Geophysical Research*, *113*, A05301. https://doi.org/10.1029/2007JA012605

Otsuka, Y., Shiokawa, K., & Nishioka, M. (2012). VHF radar observations of post-midnight *F*-region field-aligned irregularities over Indonesia during solar minimum. *Indian Journal of Radio & Space Physics*, *41*, 199–207.

Patra, A. K., Phanikumar, D. V., & Pant, T. K. (2009). Gadanki radar observations of *F* region field-aligned irregularities during June solstice of solar minimum: First results and preliminary analysis. *Journal of Geophysical Research*, *114*, A12305. https://doi.org/10.1029/2009JA014437

Pi, X., Mannucci, A. J., Lindqwister, U. J., & Ho, C. M. (1997). Monitoring of global ionospheric irregularities using the worldwide GPS network. *Geophysical Research Letters*, *24*(18), 2283–2286. https://doi.org/10.1029/97GL02273

Rastogi, R. G. (1980). Seasonal and solar cycle variations of equatorial spread *F* in the American sector. *Journal of Atmospheric and Terrestrial Physics*, *42*(7), 593–597. https://doi.org/10.1016/0021-9169(80)90093-8

Rastogi, R. G., & Chandra, H. (2015). Spread F at tropical latitude stations in India. *Indian Radio and Space Physics*, *44*, 177–186.

Ray, S., & DasGupta, A. (2007). Geostationary L-band signal scintillation observations near the crest of equatorial anomaly in the Indian zone. *Journal of Atmospheric and Terrestrial Physics*, *69*(4-5), 500–514. https://doi.org/10.1016/j.jastp.2006.09.007

Ren, Z., Wan, W., Liu, L., Chen, Y., & Le, H. (2011). Equinoctial asymmetry of ionospheric vertical plasma drifts and its effect on *F*-region plasma density. *Journal of Geophysical Research*, *116*, A02308. https://doi.org/10.1029/2010JA016081

Rodrigues, F. S., Crowley, G., Heelis, R. A., Maute, A., & Reynolds, A. (2012). On TIE-GCM simulation of the evening equatorial plasma vortex. *Journal of Geophysical Research*, *117*, A05307. https://doi.org/10.1029/2011JA017369

Sastri, J. H. (1998). On the development of abnormally large postsunset upward drift of equatorial *F* region under quiet geomagnetic conditions. *Journal of Geophysical Research*, *103*(A3), 3983–3991. https://doi.org/10.1029/97JA02649

Sastri, J. H. (1999). Post-midnight onset of spread-*F* at Kodaikanal during the June solstice of solar minimum. *Annales de Geophysique*, *17*, 1111–1115.

Sastri, J. H., Abdu, M. A., Batista, I. S., & Sobral, J. H. A. (1997). Onset conditions of equatorial (range) spread *F* at Fortaleza, Brazil, during the June solstice. *Journal of Geophysical Research*, *102*(A11), 24,013–24,021. https://doi.org/10.1029/97JA02166

Sripathi, S., Bose, S., Patra, A. K., Pant, T. K., Kakad, B., & Bhattacharyya, A. (2008). Simultaneous observations of ESF irregularities over Indian region using radar and GPS. *Annales de Geophysique*, *26*(11), 3197–3213. https://doi.org/10.5194/angeo-26-3197-2008

Sripathi, S., Kakad, B., & Bhattacharyya, A. (2011). Study of equinoctial asymmetry in the equatorial spread *F* (ESF) irregularities over Indian region using multi- instrument observations in the descending phase of solar cycle 23. *Journal of Geophysical Research*, *116*, A11302. https://doi.org/10.1029/2011JA016625

Stephan, A. W., Colerico, M., Mendillo, M., Reinisch, B. W., & Anderson, D. (2002). Suppression of equatorial spread *F* by sporadic *E*. *Journal of Geophysical Research*, *107*(A2), 1021. https://doi.org/10.1029/2001JA000162

Subbarao, K. S. V., & Murthy, B. V. K. (1994). Seasonal variations of equatorial spread-*F*. *Annales de Geophysique*, *12*(1), 33–39, https://doi.org/10.1007/s00585-994-0033-4.

Taori, A., Parihar, N., Ghodpage, R., Dashora, N., Sripathi, S., Kherani, E. A., & Patil, P. T. (2015). Probing the possible trigger mechanisms of an equatorial plasma bubble event based on multistation optical data. *Journal of Geophysical Research: Space Physics*, *120*, 8835–8847. https://doi.org/10.1002/2015JA021541

Tiwari, P., Tiwari, D., Surve, G., & Nayak, C. (2012). Sporadic E over Allahabad during the extremely prolonged low solar activity period of 2007–2009. *Indian Journal of Radio & Space Physics*, *41*, 285–293.

Tsunoda, R. T. (2007). Seeding of equatorial plasma bubbles with electric fields from an Es-layer instability. *Journal of Geophysical Research*, *112*, A06304. https://doi.org/10.1029/2006JA012103

Tsunoda, R. T., & Ecklund, W. L. (2007). On the post-sunset rise of the equatorial *F* layer and superposed upwellings and bubbles. *Geophysical Research Letters*, *34*, L04101. https://doi.org/10.1029/2006GL028832

Tulasi Ram, S., Rama Rao, P. V. S., Niranjan, K., Prasad, D. S. V. V. D., Sridharan, R., Devasia, C. V., & Ravindran, S. (2006). The role of post-sunset vertical drifts at the equator in predicting the onset of VHF scintillations during high and low sunspot activity years. *Annales de Geophysique*, *24*(6. Copernicus GmbH, 2006), 1609–1616. https://doi.org/10.5194/angeo-24-1609-2006

Uemoto, J., Maruyama, T., Saito, S., Ishii, M., & Yoshimura, R. (2010). Relationships between pre-sunset electrojet strength, pre-reversal enhancement and equatorial spread-*F* onset. *Annales de Geophysique*, *28*(2), 449–454. https://doi.org/10.5194/angeo-28-449-2010

Whalen, J. A. (2002). Dependence of equatorial bubbles and bottomside spread *F* on season, magnetic activity, and $\mathbf{E} \times \mathbf{B}$ drift velocity during solar maximum. *Journal of Geophysical Research*, *107*(A2), 1024. https://doi.org/10.1029/2001JA000039

Yizengaw, E., Retterer, J., Pacheco, E. E., Roddy, P., Groves, K., Caton, R., & Baki, P. (2013). Postmidnight bubbles and scintillations in the quiet-time June solstice. *Geophysical Research Letters*, *40*, 5592–5597. https://doi.org/10.1002/2013GL058307

Yokoyama, T., Pfaff, R. F., Roddy, P. A., Yamamoto, M., & Otsuka, Y. (2011). On postmidnight low-latitude ionospheric irregularities during solar minimum: 2. C/NOFS observations and comparisons with the Equatorial Atmosphere Radar. *Journal of Geophysical Research*, *116*, A11326. https://doi.org/10.1029/2011JA016798

Yokoyama, T., Yamamoto, M., Otsuka, Y., Nishioka, M., Tsugawa, T., Watanabe, S., & Pfaff, R. F. (2011). On postmidnight low-latitude ionospheric irregularities during solar minimum: 1. Equatorial Atmosphere Radar and GPS-TEC observations in Indonesia. *Journal of Geophysical Research*, *116*, A11325. https://doi.org/10.1029/2011JA016797